RSC Advances

ROYAL SOCIETY OF CHEMISTRY

www.rsc.org/advances

Influence of Aliovalent Cation substitution on structural and electrical properties of $Gd_2(Zr_{1-x}M_x)_2O_{7-\delta}$ (M = Sc, Y) system

Vaisakhan Thampi D. S., Prabhakar Rao Padala[*], Renju U. A.

Materials Science and Technology Division, National Institute for Interdisciplinary Science

and Technology (NIIST), Trivandrum, India-695019

*Corresponding author. Tel.: + 91 471 2515311; Fax: + 91 471 2491712
E-mail: padala_rao@yahoo.com

Abstract:

Fluorite-type zirconate compositions of the form $Gd_2(Zr_{1-x}M_x)_2O_{7-\delta}$ (M = Sc and Y; $x = 0$, 0.1,

0.2, 0.3, 0.4) were prepared by a solid state reaction route and the influence of aliovalent

cation substitution on the structural and electrical properties were investigated using Powder

X-ray diffraction, Raman spectroscopy, transmission and scanning electron microscopy and

impedance spectroscopy techniques. Despite being in the same group of elements, the two

substituent cations introduced oxygen vacancies with contrasting influence on the parent

lattice and ionic conductivity. Larger ionic radius of Y^{3+} forced the lattice to expand which

along with the increased anion defects lowered the energy barrier for charge transport

enhancing the ionic conductivity. Whereas, in Sc-substituted compositions, oxygen vacancies

dominated over ionic size causing the lattice to contract and their cooperative behavior turned

out to be disadvantageous for long range conduction process with increased activation energy

resulting in lowering the ionic conductivity. The changes in rigidity of the inter-ionic bonds

and the lattice volume introduced by the substituent cations also influenced the thermal

expansion behavior of the materials. This work demonstrates that the influence of oxygen

vacancies on the ionic conductivity is also dependent on the size of aliovalent substituent ion.

Keywords: Gadolinium zirconate; Solid oxide electrolyte; Impedance Spectroscopy; Electrical conductivity

Introduction

On the backdrop of diminishing energy resources, a quest for efficient solid oxide electrolyte materials to be used for fuel cell applications have been going on since the last few decades. Electrolyte is the heart of a solid oxide fuel cell.[1] Since fuel cells constitute a promising category of non-conventional energy resources, material development for them, especially electrolytes, has gained much attention.[2, 3] The electrolyte materials should possess some specific features like high electrical conductivity, adequate thermal and mechanical properties like strength, creep, etc., thermodynamic and structural stability.[4] Apart from this, properties like thermal expansion should match with the other fuel cell components, which poses limitations in changing to completely new ceramic systems.[1]

Various zirconate ceramics having a general formula $A_2B_2O_7$ have been studied extensively in this respect wherein attempts to enhance the electrical properties have been made by means of substitution or addition of foreign cations in already known chemical systems.[5-9] These zirconate compositions mostly crystallize in either a pyrochlore-type or a fluorite-type lattice depending on the difference in size between the two cations.[10] The larger the ionic size difference, higher will be the structural order within the lattice and the ordering or disordering transitions between the two structures induced by cation-substitution are found to have some influence on the electrical properties of these compounds.[11-13] Among the various zirconate systems reviewed, $Gd_2Zr_2O_7$ is reported to be one of the best with respect to the electrical characteristics.[14-16] It is known to exist both in fluorite and pyrochlore structures with various preparation conditions.[17] There have also been many attempts to tailor the properties of this chemical system with varying results, some being positive and some

negative.[14-16, 18-20] Substitution of Gd^{3+} by Sm^{3+} and then co-substitution by Ca^{2+} had positive effects on the properties of parent composition.[19, 21] Substitution by Eu^{3+} also was helpful for improved electrical properties.[16] Nb^{5+} while substituting Zr^{4+} led to an enhancement in the electrical conductivity whereas Ce^{4+} and Mo^{6+} in that place were found to bring it down.[15, 20, 22] In most of these studies, there were certain optimum levels of substitution that corresponded to the maximum value of conductivity, which depended on many other factors like lattice order, lattice volume, point defects, etc. Thus, despite extensive attempts, there does not exist any general rule that can guide to the best direction to achieve desired properties.

Since defect-fluorite structures involve more than one type of cations, they can inherently contain some amount of order. Most of the aforementioned substitution attempts are focused on the A-cation site. Here in the present work two cations, Sc^{3+} and Y^{3+}, were independently chosen to substitute the Zr^{4+} partially in the B-site of $Gd_2Zr_2O_7$. The differences in ionic size can influence the crystal order and the lattice volume. That, along with the difference in valence, was expected to influence various physical properties. Crystal structure and electrical properties were given prime focus in the present investigation. The independent substitution would help to contrast between ions and to understand the various mechanisms distinctly.

Experimental

Solid solutions of general formula $Gd_2(Zr_{1-x}M_x)_2O_{7-\delta}$ (M = Sc, Y; x = 0, 0.1, 0.2, 0.3, 0.4) were prepared. Conventional solid state reaction route involving choice of oxides of the cations as reactants and wet mixing followed by heat treatment was adopted for the synthesis of the samples. Homogenous mixture of Gd_2O_3 (Aldrich, 99.9%), ZrO_2 (Aldrich, 99%), Sc_2O_3 (Alfa Aesar, 99.99%) and Y_2O_3 (Sigma-Aldrich, 99.99%) weighed according to

stoichiometry was calcined at 1300°C and recalcined at 1600°C, both for 6 h each. The product powders were then made to green pellets with a hydraulic press applying uniaxial compaction at 2.5 MPa. The pellets were then sintered at 1650°C for 24 h.

The prime tool to investigate structural features was an X-ray diffractometer (X'Pert Pro, PANalytical) making use of Cu Kα radiation of wavelength 1.54 Å. The diffractograms were recorded in a 2θ range of 10° to 90°. FT-Raman spectra of samples were obtained by exciting with an argon laser of wavelength 784 nm using a Labram HR 800 spectrometer (Horiba Scientific). Morphological features were examined through electron microscopic technique, namely a scanning electron microscope (SEM, model: JEOL JSM-5600LV) and a transmission electron microscope (TEM, TECNAI 30G2 S-TWIN, the Netherlands), which were also helpful in confirming the crystallinity of prepared samples. The response of the crystals to high temperature was analyzed through high-temperature X-ray diffraction (Anton-Paar High-temperature attachment to XRD). Impedance spectroscopy was used to probe the electrical properties. Cylindrical pellets were subjected to two-point impedance measurement using an impedance analyzer (Solartron SI 1260) through a dielectric interface (Solartron 1296). Electroding was done at polished end-faces painted with silver-paste and the measurement frequency was varied from 1 MHz to 1 Hz, in a temperature range of 473 K to 1023 K.

Results and Discussion

In coming sections, the Sc^{3+} and Y^{3+} substituted samples of the form $Gd_2(Zr_{1-x}M_x)_2O_{7-\delta}$ (M = Sc, Y; $x = 0, 0.1, 0.2, 0.3, 0.4$) will be respectively labelled with the codes GZS and GZY with a numeral representing the value of x for each sample. GZ will stand for $Gd_2Zr_2O_7$.

Crystal structure

Powder X-ray diffraction was made use of to understand the maximum feasibility of solid solution formation and to analyze the crystal structure of the synthesized materials. Sharp X-ray reflections could be seen in the recorded diffraction pattern that indicated the crystalline nature of the samples. A comparison with standard ICDD powder pattern No. 01-080-0471 showed that all the single phase compositions crystallized in a cubic fluorite-type structure with Fm3m space group.
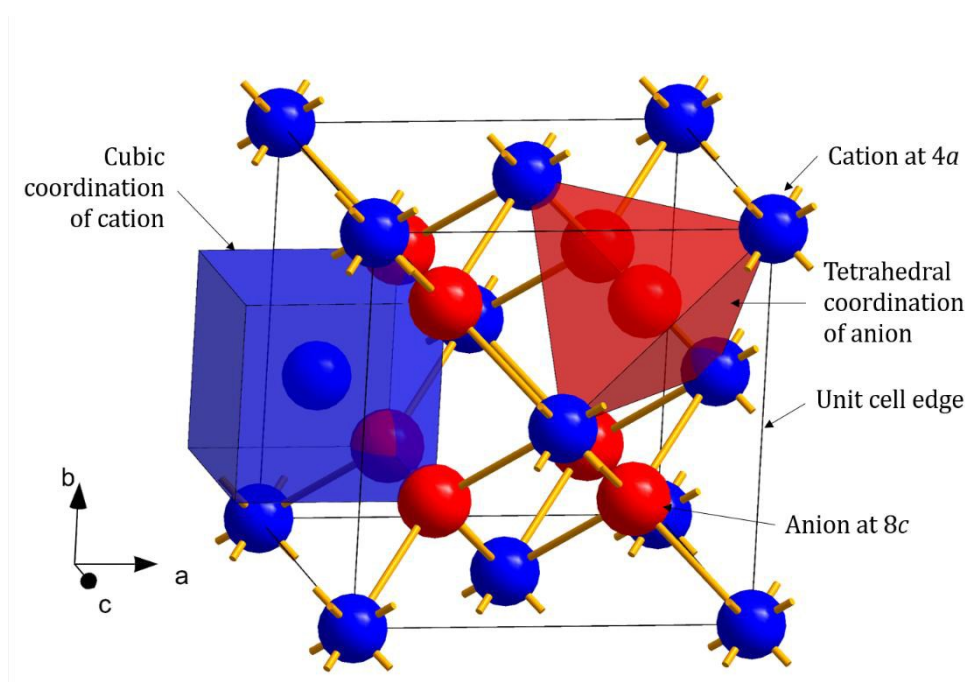

Figure1: Cubic fluorite structure. Blue spheres represent cations and red spheres represent anions. The polyhedra represent the coordination environments of both species.

In the cubic fluorite-type crystals, the cations constitute a face centered lattice and are cubically coordinated by eight anions as shown in figure 1. The anions, whereas, are coordinated by four cations which form a tetrahedron about each of them. The crystallographically different lattice positions are designated by Wyckoff notations $4a$ (0, 0, 0) and $8c$ (0.25, 0.25, 0.25) occupied respectively by cations and anions. In $Gd_2Zr_2O_7$, which is considered to be a defect fluorite-type crystal, the Gd and Zr ions are disordered over an

fcc lattice. The XRD patterns of the $Gd_2(Zr_{1-x}M_x)_2O_{7-\delta}$ compositions are shown in figure 2 and 3. It could be observed that the $Gd_2Zr_2O_7$ lattice accommodated the aliovalent M ion (M = Sc^{3+}, Y^{3+}) in the Zr^{4+} site to a fairly good extent of $x = 0.3$. Although both Sc^{3+} and Y^{3+} showed maximum solubility in solid solution formation at $x = 0.3$, a close observation of the peak patterns showed that the overall influence the substitution had on the crystal structure was different from one another.
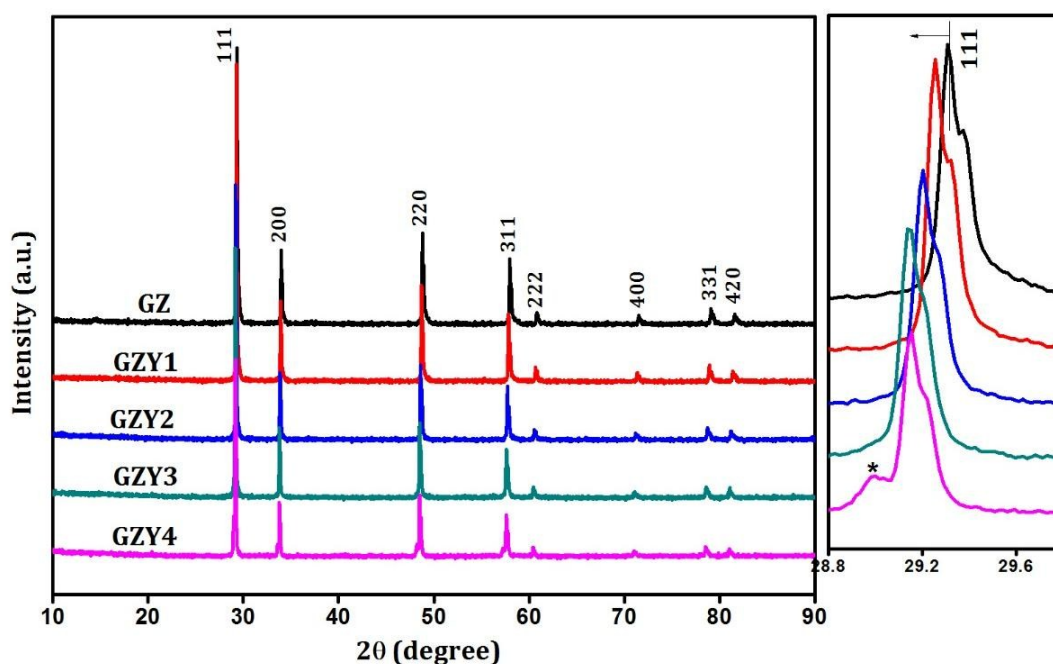

Figure 2: Powder X-ray diffraction patterns of $Gd_2(Zr_{1-x}Y_x)_2O_{7-\delta}$. Side panel shows the expanded view of (111) peak.

With substitution of Zr^{4+} by Y^{3+}, the X-ray reflections were found to shift towards lower angles as seen in the side panel of figure 2, indicating an increase in the interplanar spacing of various miller planes. But the trend observed for substitution by Sc^{3+} was different, and there the reflections moved towards higher angles (as in figure 3) with increasing amount of substitution. In both cases there was no appreciable change in the width of diffraction peaks.
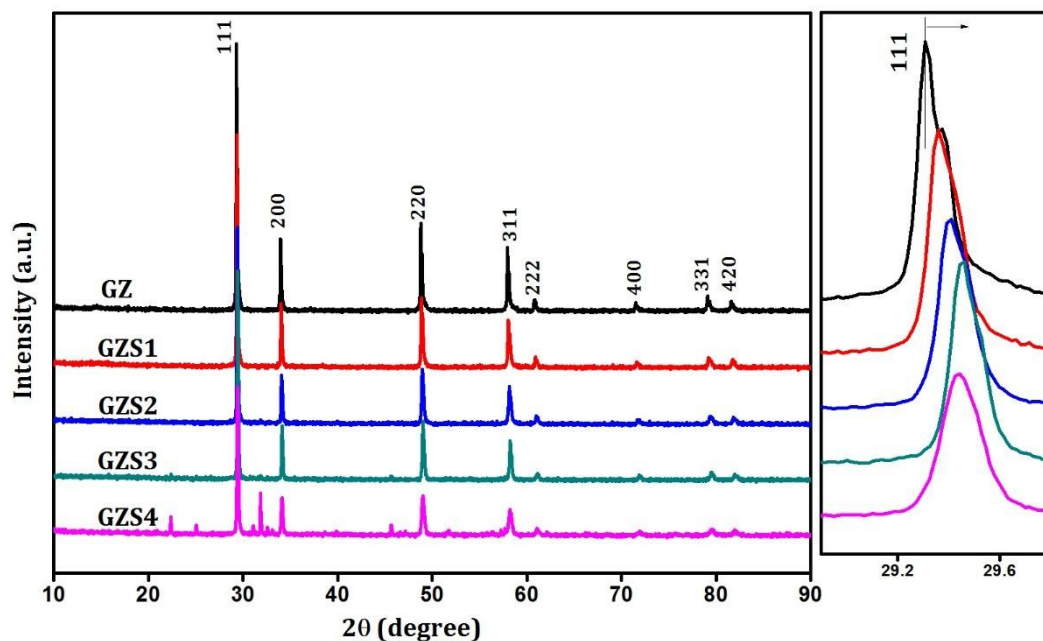
Figure 3: Powder X-ray diffraction patterns of Gd$_2$(Zr$_{1-x}$Sc$_x$)$_2$O$_{7-\delta}$. Side panel shows the expanded view of (111) peak

A more detailed and quantitative analysis of the XRD data was carried out by Rietveld

simulation and refinement method using commercially available X'pert Highscore plus[23]

software. A standard peak-matching procedure with the ICDD crystal structure database

helped constructing starting models for pattern simulation, with the stoichiometry providing

an intuitive idea about the ionic occupancies. Fitting of diffraction peaks demanded a pseudo-

Voigt line profile function which is essentially a linear combination of Gaussian and

Lorentzian functions. The Caglioti parameters, flat background and two background function

coefficients were chosen for refinement along with the unit cell identities. Various refinement

parameters including the agreement indices are listed in Table 1.

Table 1: Important results from Rietveld analysis (Refined fitting parameters are presented in SI, Table S1)

	GZ	GZY1	GZY2	GZY3	GZY4	GZS1	GZS2	GZS3
Unit cell	Cubic	Cubic	Cubic	Cubic	Cubic	Cubic	Cubic	Cubic
Space group	Fm3m	Fm3m	Fm3m	Fm3m	Fm3m	Fm3m	Fm3m	Fm3m
Scale Factor	0.000181	0.000187	0.000158	0.000161	0.000133	0.000181	0.000175	0.000164
Cell a [Å]	5.2729(1)	5.2831(1)	5.2932(1)	5.3011(1)	5.3028(2)	5.2659(1)	5.2581(1)	5.2516(1)
R$_p$(%)	6.45	6.23	6.15	6.02	6.91	6.04	5.48	5.84

$R_{exp}(\%)$	6.76	6.63	6.88	6.84	7.21	6.89	7.15	7.13
$R_{wp}(\%)$	9.2	8.65	7.93	7.64	8.97	7.9	7.01	7.43
GOF	1.87	1.7	1.32	1.24	1.54	1.31	0.96	1.08

It can be observed from the result of Rietveld refinement that the influence on the fundamental lattice vector of the $Gd_2Zr_2O_7$ lattice is different for Sc and Y ions. While considering the lattice volume in substitution processes, the most commonly reported influence comes from the radius of the substituent ion. According to Vegard's law[24], a larger ion substituting a smaller ion is expected to increase the lattice volume and vice versa. The ionic radii of Gd^{3+}, Zr^{4+}, Sc^{3+} and Y^{3+} under the eight-coordination condition in a fluorite type lattice are 1.053 Å, 0.84 Å, 0.87 Å and 1.019 Å respectively.[25] Although both these substituent cations are larger in radius than Zr^{4+}, substitution by Sc^{3+} decreases the effective lattice parameter while substitution by Y^{3+} increases it.

For Y^{3+} substitution, the incorporation of larger ions into the $4a$ sites previously occupied by smaller Zr^{4+} ions forces the lattice to expand. This is evident in figure 4(a) where there is a linear increase in the lattice parameter with increase in Y^{3+} substitution. For the GZY4 sample, the peak is seen to swerve from this trend. This may be because, beyond the limit of solubility, substituent ions tend to form other impurity phases without causing much strain to the parent lattice. The last data point of the lattice parameter plot in figure 4(a) illustrates this, where the increase in lattice parameter beyond $x = 0.3$ is comparatively very less.
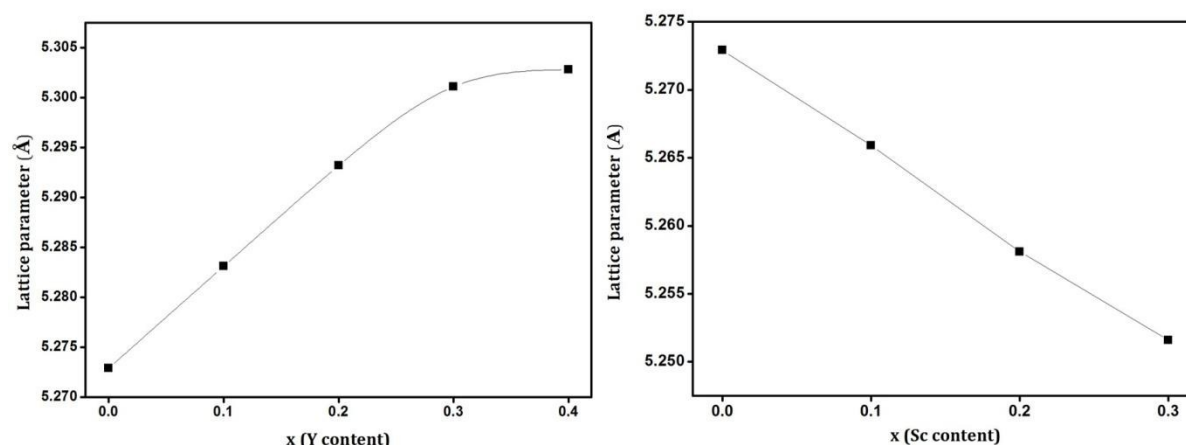
Figure 4: Variation of lattice parameter with substitution for (a) GZY series (b) GZS series

On the contrary, the lattice parameter is decreasing substitution by Sc^{3+} as evident in figure

4(b). This may be attributed to the effect of Schottky defects in the anionic sublattice caused

by aliovalent substitution. When tetravalent Zr is substituted by trivalent Sc, oxygen

vacancies will be created in the lattice for electrostatic balance. Substitution of every two Zr

ions will create one oxygen vacancy in the vicinity, and can be represented in Kroger-Vink

notation as

$$2Zr^{4+} \rightarrow 2M^{3+} + V_o^{\cdot\cdot}$$
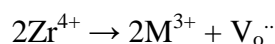
This will reduce the average coordination number of the 4*a* site cation which is 8 for an ideal

fluorite-type lattice. Marrochelli et al. established through molecular dynamics simulation

and a meta-analysis of literature that the size of an oxygen vacancy is smaller than an oxygen

ion.[26] They report that for host cations smaller than Ce^{4+} in fluorite-structure, the asymmetric

cation relaxations around an oxygen vacancy can lead to a significant contraction of the

lattice.[27] This is observed by the shift of X-ray reflection peaks towards higher angles. Such

an effect has been observed in some other similar chemical systems too.[28, 29] A close

examination of the XRD patterns showed that there is no considerable change in the width of

diffraction peaks with respect to both substitutions. Instrumental broadening, crystallite size

effect and lattice strain are the key factors that contribute to the line width in diffraction

pattern. Since the first two factors were made as equivalent as possible for all the samples through same measurement conditions and similar crystallite sizes, any change in the line width could be loosely attributed to the lattice strain. Absence of such an effect may be indicating that the substitution process does not introduce much strain to the lattice. In this context, it is reasonable to assume that when the cationic size difference is comparatively smaller, the effect of oxygen vacancies becomes dominant as far as substitution by Sc^{3+} and Y^{3+} are compared.

A parallel way to understand the structural influence of the ionic substitution was attempted through FT-Raman analysis. In the cubic fluorite structure, the site symmetry of the 4a site cation is O_h and that of the 8c anion is T_d.[30] Factor group analysis had shown that an ideal cubic fluorite lattice would possess only one Raman active mode T_{2g} which is generally found at ~470 cm^{-1}.[31-33]
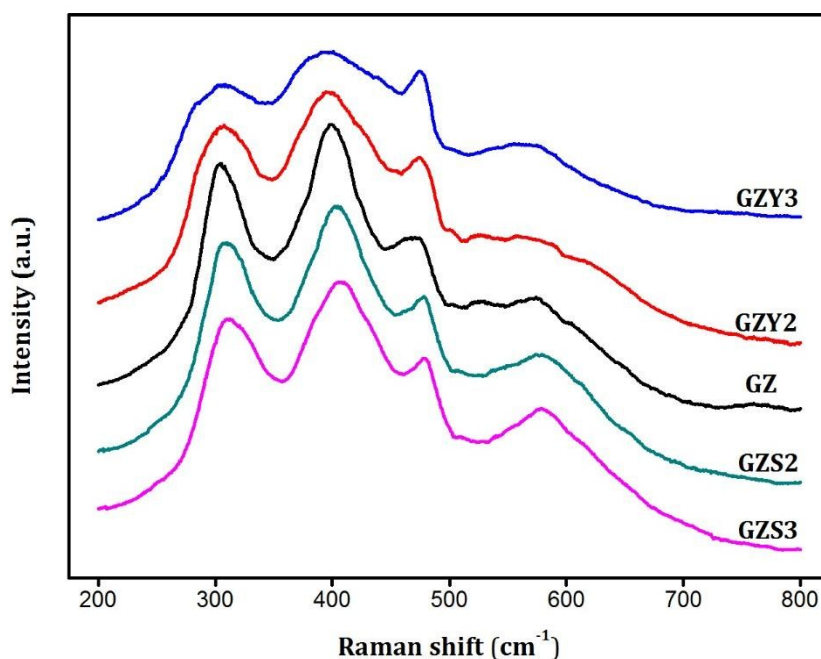

Figure 5: FT-Raman spectra showing the effect of cation substitution.

However in figure 5, more than one peak could be distinguished in the Raman spectra which are generally broad in nature. The broad nature of Raman modes cannot be a result of small

crystallite size since the sharp X-ray reflections and the images in the SEM and TEM

analyses indicate the contrary. The broadness is a result of inherent deviations from the

translational periodicity in the lattice of a disordered fluorite structure.[34-36] Presence of some

additional vibrations below and above the T_{2g} frequency can be justified by acknowledging

the deviation of the present system from an ideal fluorite lattice. In such defect fluorite-type

crystals some degree of ordering will always be present due to the different cations occupying

the same crystallographic site and this is expected to give rise to some additional vibrational

modes as visible in figure 5.[31, 33] As observed in the present system, T_{2g} mode in defect

fluorites is reported to be generally very weak and broad in nature.[12, 37] Broadening of

vibrational modes is often an indication of increasing disorder in a crystal lattice. The

cationic size difference is a crucial factor deciding the extent of order in fluorite-related

structures like pyrochlores. In pyrochlore type structures with a general formula $A_2B_2O_7$, the

ratio of radii of A and B cations (r_A/r_B) gives a measure of order. In the discussions regarding

the order-disorder transitions in such chemical systems, ordered pyrochlore structure is said

to be stable in the r_A/r_B range of 1.76 to 1.46 and a decrease in r_A/r_B is a driving factor of

disorder.[11, 38, 39] Considering the size of the cations involved in the present system, it can be

inferred that substitution by Sc and Y, both being larger than Zr and smaller than Gd, would

in effect bring down the cationic size difference in the lattice thereby leading to more

disorder. This can be understood from the observation that Y^{3+} substituted system, it being

the larger of the two substituent cations, show more broadening than the Sc^{3+} substituted

one.[34]

A contrast between two substitutions is seen when the peak position is analyzed. With Sc-

substitution, the T_{2g} mode is found to show a small positive shift in frequency whereas with

Y-substitution it is showing a small negative shift. McBride et. al[32] had observed and

explained a positive frequency shift of Raman modes in fluorite structure due to the

formation of oxygen vacancies in the lattice. According to their model oxygen vacancies can give rise to another peak at ~570 cm^{-1} which was later reported by Li et. al also.[33] A small hump can be observed in our Sc substituted system too, at an adjacent frequency, which can be interpret to emphasize the dominance of oxygen vacancies in deciding the structural properties of those chemical compositions. A small negative shift of vibrational modes in Y substituted compositions can be attributed to the increase in lattice volume caused by the considerably larger substituent cation.[32]

Thermal expansion behavior

High-temperature X-ray diffraction study was carried out to investigate the response of the crystal lattice to change in temperature. Powder XRD patterns of various samples were recorded at intervals of 200 degrees from 298 K to 1273 K and the evolution of various structural features were observed. These materials retained their crystallinity and crystal structure at all measuring temperatures and did not show any structural transition.

The effect of increase in temperature is reflected in two aspects of the X-ray diffraction peak; position and intensity (Data of a representative sample is illustrated in SI, figure S1). As the temperature increases from 298 K towards 1273 K, the peaks progressively shift towards lower diffraction angles and at the same time their intensity dwindle. The shift of peaks is quite obvious since the phonon frequencies in real crystals depend on the amplitude of lattice vibrations hence making the phonon gas pressure a temperature-dependent parameter. The ultimate reason for this is the anharmonic nature of lattice potential which in a vast majority of real crystals lead to an expansion of linear dimensions with increase in temperature. Thus the progressive shift of X-ray diffraction peaks towards lower angles is the direct indication of thermal expansion behavior.

The decrease in peak intensity can be explained by the effect of lattice vibrations on the coherent scattering of X-rays from the crystal. As the prime role in X-ray scattering from a crystal is played by the electron cloud around various atoms, the vibration of atoms about their equilibrium positions has an effect of smearing the electron cloud into larger volumes in effect bringing about a decrease in electron charge density. Thus, the increase in vibration amplitude with increase in temperature should lead to a decrease in scattering intensity. This effect has been formulated as the Debye-Waller factor (DWF) that appears as an exponential term in the theoretical expression for Bragg peak intensity.[40] The concept of DWF is quite involved and its calculation warrants more sophisticated instrumentation.[41] Even then, it is reasonable to assume that the rate of decrease of intensity is connected to the rigidity of the lattice, since the amplitude of atomic vibrations are dependent on it. It is observed that the Sc-substituted samples are more susceptible to loss of scattering intensity with respect to temperature (See figure S2 in SI). With increase in Y-substitution the rate of decrease in intensity shows a decrease. This can be an indication of increase in rigidity of the lattice.
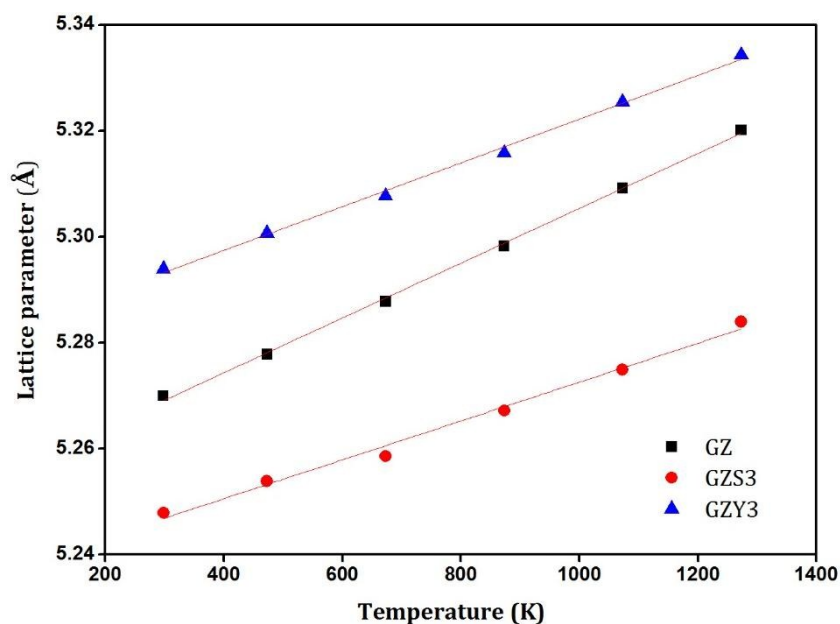

Figure 6: Lattice parameter vs temperature plot for three representative samples

The recorded X-ray diffraction patterns of all the samples at all temperatures were analyzed by carrying out Le-Bail fitting using X'Pert HighScore plus software which yielded the corresponding lattice parameter values. Lattice parameter showed a linear increase with temperature as shown in figure 6. The slope of the respective plots could be used to calculate their thermal expansion coefficient through the equation,

$$\alpha = 1/a_{298}(\mathrm{d}a/\mathrm{d}T) \ \mathrm{K}^{-1} \ \text{-------- (1)}$$

where α is the thermal expansion coefficient (TEC), a_{298} is the original lattice parameter measured at room temperature and $\mathrm{d}a/\mathrm{d}T$ is the slope of the lattice parameter variation with respect to temperature.
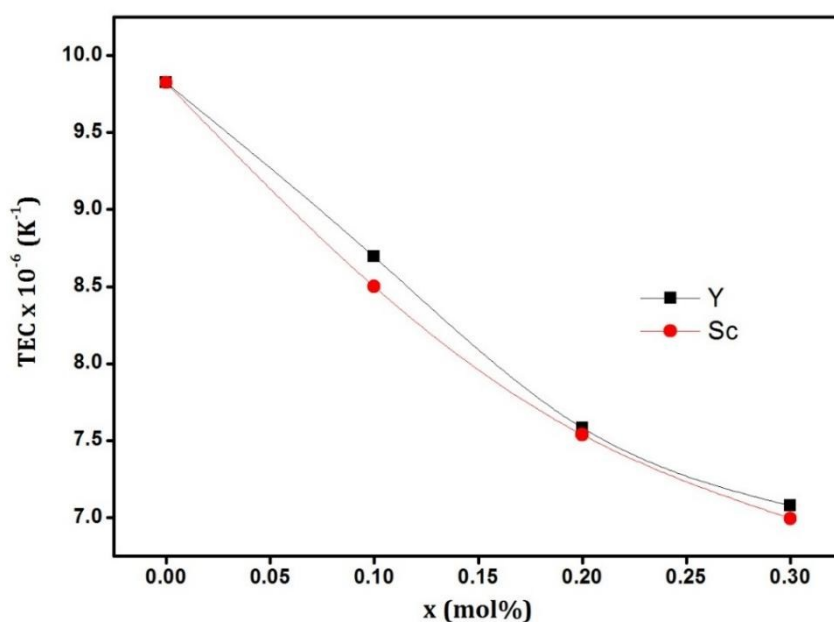

Figure 7: Variation of thermal expansion coefficient (TEC) with substitution.

Effect of cationic substitution on the thermal expansion behavior is reflected in the plot of TEC against the substituent mole fraction (x), as shown in figure 7. It can be seen that the TEC decreases with increase in substitution for both Sc and Y. Although both cations

introduce the same effect, the mechanisms through which these effects are brought about seem to be different. The decrease in TEC with Y-substitution can be explained by the change in ionic nature of the average diatomic bonds in the crystal. The electronegativity of Zr, Sc, Y and O in Pauling scale are 1.33, 1.36, 1.22 and 3.44 respectively.[42] Since the ionic nature, and hence the strength of bonding, is proportional to the difference in electronegativities of the participant atoms, substitution of Zr atoms by less electronegative Y atoms is going to increase the ionic nature of the average diatomic bond in the crystal. This will increase the ionization energy of the electrons involved in the bonding process which is connected to the phonon frequency. There exists a theoretical proof that the square of the phonon frequency is directly proportional to the exponential of the ionization energy of the bond-forming electrons.[43] Hence in the Y-substitution scenario of the present system, the phonon frequency is expected to increase thereby making the lattice more rigid. This can explain the decrease in thermal expansion coefficient. But in the case of Sc-substitution, direct influence of ionic nature is not seen since, Sc being more electronegative than Zr should in that case increase the TEC. The reverse trend observed here may be attributed to the oxygen vacancies. As we have noted the dominance of oxygen vacancies in Sc-substituted system, this decrease in TEC may be due to the clustering of oxygen vacancies as was earlier reported by Liu et al.[14] The lattice contraction caused by these vacancies may also contribute to this phenomenon.

Morphology:

The powder X-ray diffraction pattern serves to indicate only the average crystalline nature of a bulk sample and hence transmission electron microscopy (TEM) was used to confirm the crystallinity of the chemical systems in small domains. HR-TEM images of some representative samples are given in SI (figure S3).

The surface morphology of sintered pellets were examined using scanning electron microcopy. The SEM images of polished surfaces of three representative samples are shown in figure 8. The typical polycrystalline morphology consisted of grains varying in size, generally in 2 μm to 6 μm range. Distinct grain boundaries could be seen along with some amount of porosity.
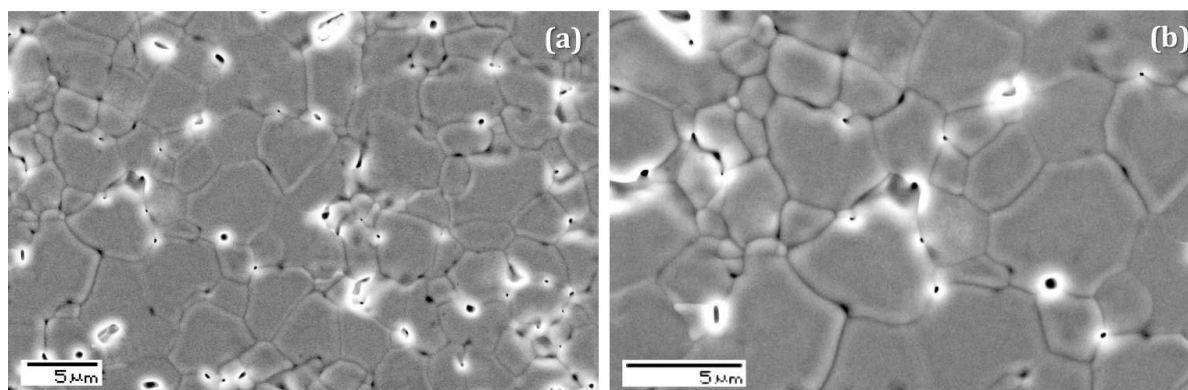

Figure 8: SEM images of the polished surfaces of two representative samples (a) GZY3 (b) GZS3

Electrical behavior:

The sintered pellets of the prepared samples were given a small ac signal (100 mV) of varying frequency (1 Hz – 1 MHz) and their response was analyzed using impedance spectroscopic technique. The measurements were made on heating conditions, from 473 K to 1023 K. A polycrystalline material in such a scenario is often considered a series of parallel RC-circuits, with the resistor (R) corresponding to conduction and the capacitor (C) corresponding to the charge accumulation effects. A Nyquist plot of imaginary part of impedance against the real part of an RC parallel circuit is a semicircle with radius R. Since the capacitance values associated with charge accumulation depends on where it happens, whether it is within the bulk of grains, in the grain boundaries or in the sample-electrode interface, the Nyquist plot for a polycrystalline material will ideally consist of three semicircular arcs.
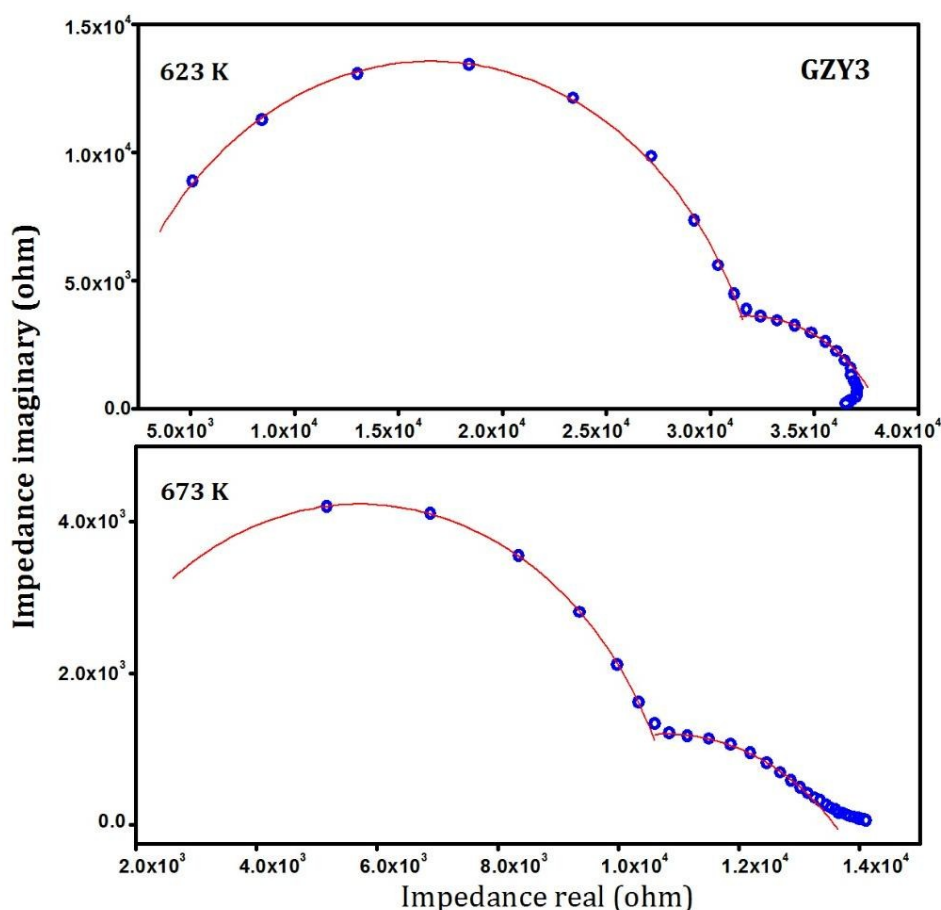
Figure 9 shows this complex plane representation of ac impedance of a representative sample, GZY3, at two different temperatures. Two semicircles could be distinguished, the mechanisms responsible for which can be identified from the capacitance values associated with them. Grain boundaries offer higher capacitance due to bigger chances of charge polarization and therefore the relaxation associated with the grain boundary phenomena falls in lower frequency region, whereas the grain relaxation happens in higher frequencies.[44] Depending on the range of measurement frequency and the difference in relaxation frequencies between grain and grain boundary phenomena, the semicircles may appear incomplete or merged as observed in figure 9. The intercept of an impedance semicircle with the real axis gives the ohmic resistance, *R*, offered against the conduction process associated with it. With increase in temperature, the semicircles diminish in radius indicating a decrease

in resistance. Considering the sample thickness (l) and the electroding area (A), the conductivity σ can be calculated as

$$\sigma = l/RA \text{ ------- (2)}$$

Since the grain and grain boundary semicircles were not always well-resolved, only their total resistance was considered to calculate the conductivity at various temperatures. The conductivity value increases with increase in temperature. This dependence is generally described by the Arrhenius equation,

$$\sigma = (\sigma_0/T)\exp(-E\text{a}/k_BT) \text{ -------- (3)}$$

where T stands for absolute temperature. E_a is the activation energy for the conduction process, σ_0 is the pre-exponential factor which is a rough measure of the availability of charge carriers and k_B is the Boltzmann constant.
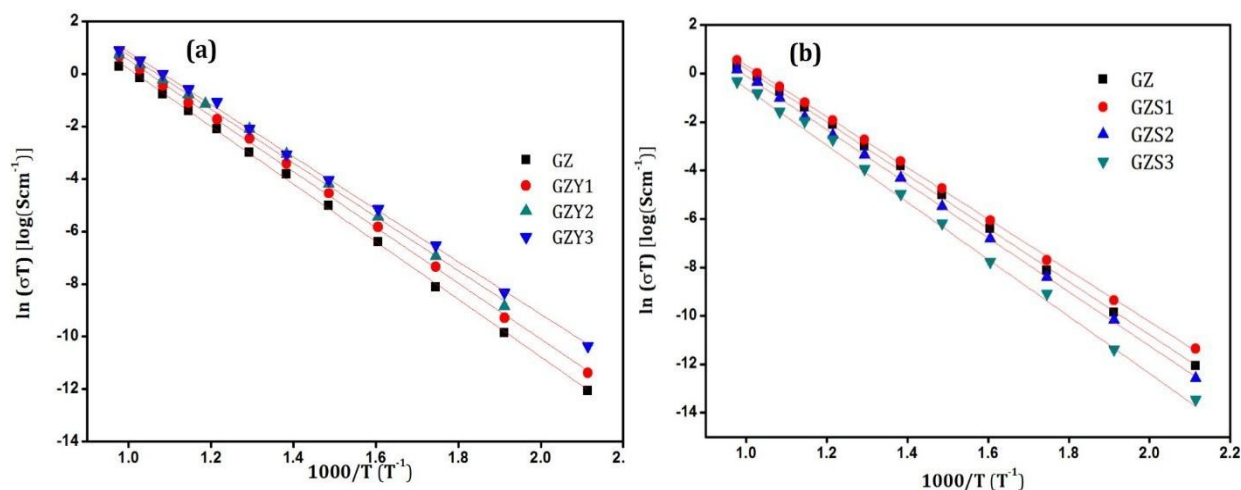

Figure 10: Arrhenius plots of various samples (a) GZY series (b) GZS series.

Figure 10 shows the Arrhenius plots of various samples, where the straight lines are the least squares fit of the conductivity data with the linearized form of equation (3). The slopes of the straight line fits would yield the values of activation energy. The values of conductivity at maximum measuring temperature (1023 K) and the activation energy of various samples are shown in figure 11.
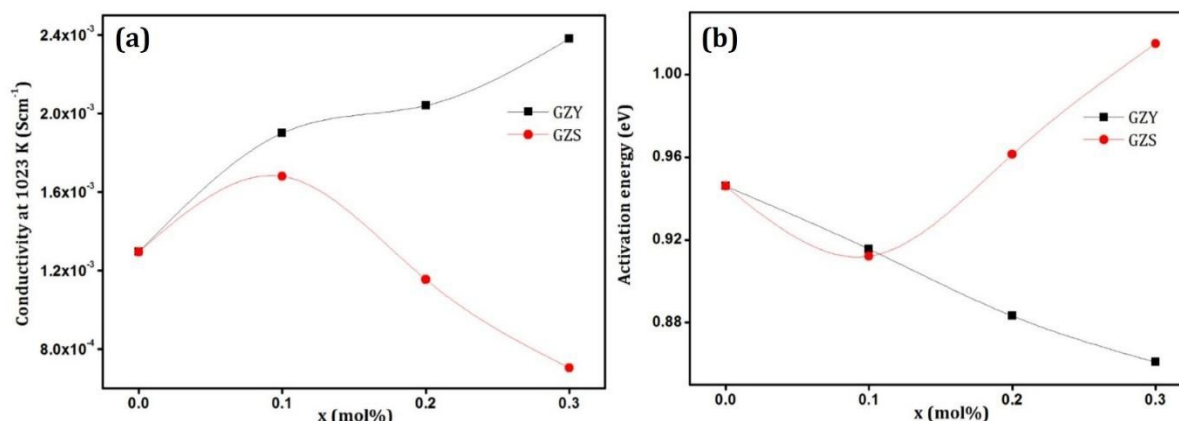

Figure 11: Effect of substitution on (a) conductivity and (b) activation energy of various samples.

It can be seen that, for GZY series, the conductivity increases with increase in substitution along with a corresponding decrease in activation energy. But in the case of GZS series, the trend is different. With substitution of Sc^{3+}, the activation energy decreases at first and then it starts to increase which reflects directly in the trend of conductivity variation also.

For a better understanding of the processes involved, analysis was extended to electric modulus function, M*, which is essentially the reciprocal of dielectric permittivity and is connected to complex impedance (Z*) as,[45]

$$M^* = j\omega C_0 Z^* \text{ ------- (4)}$$

where C_0 is the vacuum cell capacitance and ω is the frequency. The advantage of modulus formalism is that it highlights the bulk processes and does not receive much contribution from electrode polarization effects.

Figure 12 shows a frequency plot of the imaginary part (M'') of the electric modulus at various temperatures measured on the representative sample GZY3. Its value is nearly zero in the low frequency region for all temperatures, but shows a peak at a particular frequency which shifts towards higher values with increase in temperature.
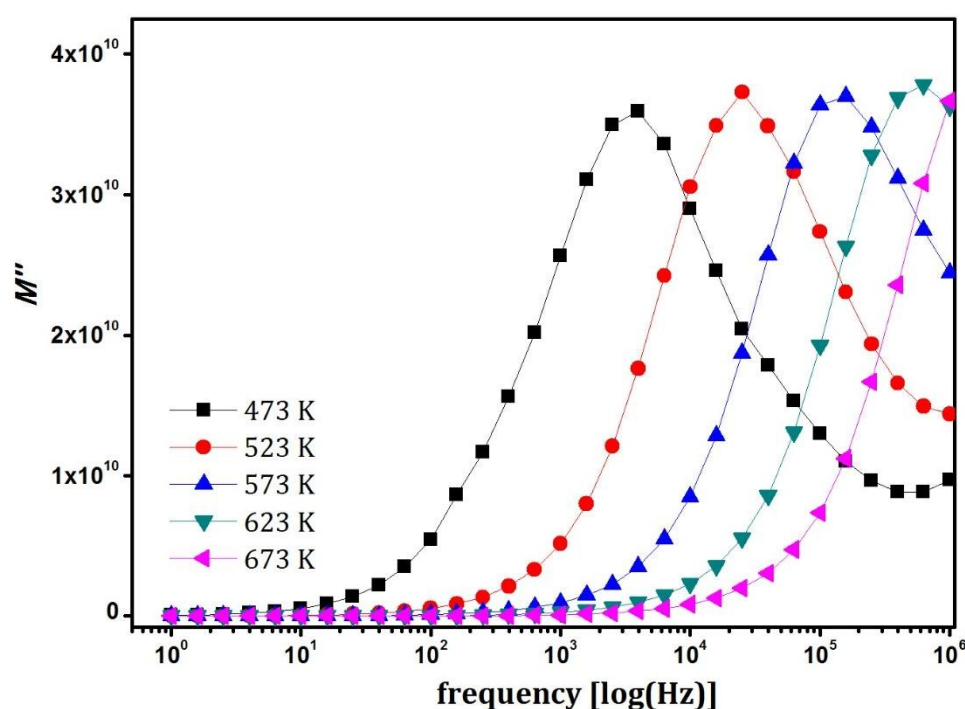

Figure 12: Frequency plot of imaginary part of electric modulus of representative sample GZY3.
The peak is obviously an indication of the dielectric relaxation behavior which in oxide ionic conductors is often attributed to the charge re-orientation of ions involving the vacancies.[46, 47] The low-frequency side of the relaxation peak corresponds to long-range conduction of ions whereas the higher frequency side to spatially confined ions.[48] The peak-shift to higher frequency implies a thermally activated ionic transport to which Arrhenius fitting is possible and activation energy could be calculated from that. The activation energies calculated from modulus and conductivity considerations were similar in values which indicated that the conduction mechanism in these materials is primarily through ion hopping.[48, 49]

The trend in conductivity as observed in figure 11 can now be explained in terms of the oxygen vacancies and the lattice disorder. The reason for enhanced conductivity in GZY series with substitution of Y^{3+} is apparently obvious. It has already been noted that both the cation substitutions are inducing a disorder to the lattice, driving the radius ratio (r_A/r_B) from 1.46 for $Gd_2Zr_2O_7$ towards 1, the value for ideal fluorite structure. This is in effect necessitating an increase in average coordination number of the cations. Y^{3+} being larger in radius compared to Sc^{3+} will be able to cooperate with this more, since it will have a larger surface area to afford the increased coordination number. Although oxygen vacancies are formed by both aliovalent substitutions, Y-substituted compositions will be able to facilitate a lower energy pathway for ionic transport within the crystal due to ease of coordination and increase in lattice volume. However, the effect of Sc^{3+} substitution in GZS series is different. Although the activation energy decreases at first due to increase in available oxygen vacancies, the system fails to keep that up for higher substituent concentration.
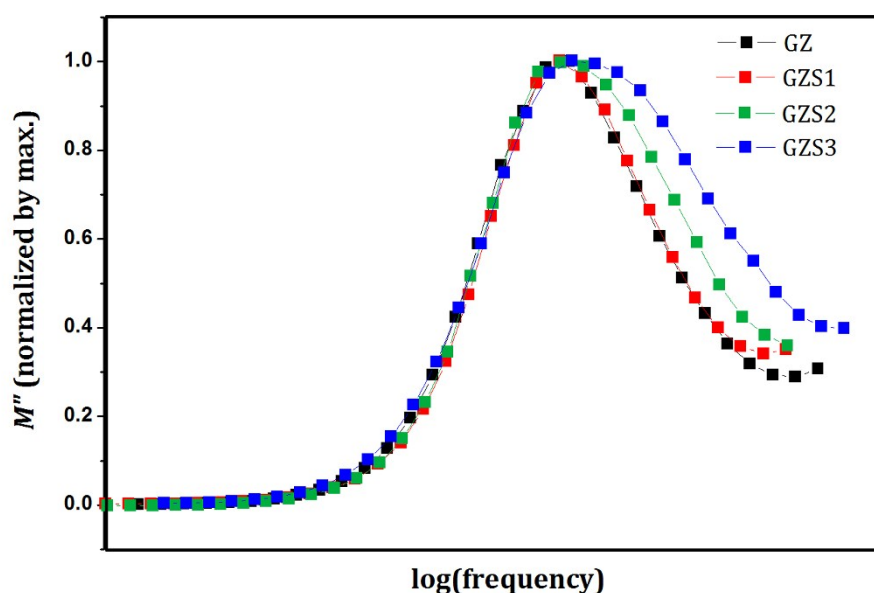

Figure 13: Broadening of modulus relaxation peak of GZS samples at 523 K. (plots were shifted along the abscissa for clarity)

It may be due to the cooperative behavior of ions in the lattice as conceived by Jonscher[50] where hopping of one ion can cause a time-dependent movement of other charge carriers in the neighborhood leading to additional relaxations. This would lead to a broadening of relaxation peaks in the modulus spectra[51, 52] as can be seen in figure 13, which shows a plot of imaginary part of electric modulus (normalized by maximum, M''/M''_{max}) of various GZS samples at 523 K. Various plots were shifted along the abscissa for clarity and beyond $x = 0.1$, a broadening of peak can be observed indicating a correlated ionic motion. This ion-ion interaction is generally reported to be detrimental to the overall electrical conductivity by posing a higher activation energy for long range ionic transport.[53] This increased cooperative behavior of oxygen vacancies in Sc-substituted compositions may be a result of the negative chemical expansion. Thus it comes out that, although Sc and Y belong to the same group, their influences on the overall behavior of the parent lattice are different from one another.

Conclusion:

$Gd_2(Zr_{1-x}M_x)_2O_7$ solid solutions were prepared to investigate the effect of substitution by M cation (M = Sc^{3+}, Y^{3+}) on structure and electrical properties. Both systems crystallized in fluorite-type lattice, showing similar extent of solid solution formation. Sc^{3+} lead to a contraction of the lattice via lattice defects, while Y^{3+} forced the lattice to expand due to its larger ionic radius. Both systems had oxygen vacancies due to aliovalent substitution, but their effect was more pronounced in the Sc-substituted compositions, as was evident in X-ray diffraction and Raman analysis. Oxygen vacancies in the expanded lattice aided in enhanced electrical properties in Y-substituted system by reducing the energy barrier for thermally activated conduction. Whereas for Sc-substituted system, cooperative behavior of ions in the contracted lattice acted in the reverse direction. Thus it could be concluded that, despite them being in the same group of *d*-block elements, the ultimate influence in physical aspects depended on the identity of the substituent ions.

References:

1.   L. Carrette, K. A. Friedrich and U. Stimming, *Fuel Cells*, 2001, **1**, 5-39.

2.   S. P. S. Badwal and K. Foger, *Ceram. Int.*, 1996, **22**, 257-265.

3.   F. M. L. Figueiredo and F. M. B. Marques, *Wiley Interdisciplinary Reviews: Energy and Environment*, 2013, **2**, 52-72.

4.   S. P. S. Badwal and F. T. Ciacchi, *Ionics*, 2000, **6**, 1-21.

5.   K. V. G. Kutty, C. K. Mathews, T. N. Rao and U. V. Varadaraju, *Solid State Ionics*, 1995, **80**, 99-110.

6.   P. J. Wilde and C. R. A. Catlow, *Solid State Ionics*, 1998, **112**, 173-183.

7.   M. Pirzada, R. W. Grimes, L. Minervini, J. F. Maguire and K. E. Sickafus, *Solid State Ionics*, 2001, **140**, 201-208.

8.   M. P. van Dijk, A. J. Burggraaf, A. N. Cormack and C. R. A. Catlow, *Solid State Ionics*, 1985, **17**, 159-167.

9.   A. J. Burggraaf, T. van Dijk and M. J. Verkerk, *Solid State Ionics*, 1981, **5**, 519-522.

10.   K. Shimamura, T. Arima, K. Idemitsu and Y. Inagaki, *Int. J. Thermophys.*, 2007, **28**, 1074-1084.

11.   M. A. Subramanian, G. Aravamudan and G. V. Subba Rao, *Prog. Solid. St. Chem.*, 1983, **15**, 55-173.

12.   A. N. Radhakrishnan, P. P. Rao, K. S. M. Linsa, M. Deepa and P. Koshy, *Dalton Trans.*, 2011, **40**.

13.   D. S. Vaisakhan Thampi, P. Prabhakar Rao and A. N. Radhakrishnan, *RSC Adv.*, 2014, **4**, 12321-12329.

14.   Z.-G. Liu, J.-H. Ouyang, Y. Zhou and X.-L. Xia, *Mater. Des.*, 2009, **30**, 3784-3788.

15.   X.-L. Xia, Z.-G. Liu, J.-H. Ouyang, S. Gao and X.-M. Liu, *Solid State Sci.*, 2011, **13**, 1328-
       1333.

16.   X.-L. Xia, J.-H. Ouyang and Z.-G. Liu, *J. Am. Ceram. Soc.*, 2010, **93**, 1074-1080.

17.   Y. H. Lee, H. S. Sheu, J. P. Deng and H. C. I. Kao, *J. Alloy. Compd.*, 2009, **487**, 595-598.

18.   L. Zhan-Guo, O. Jia-Hu, Z. Yu and X. Xiao-Liang, *Ceram. Int.*, 2009, **35**.

19.   Z.-G. Liu, J.-H. Ouyang, Y. Zhou and X.-L. Xia, *J. Power Sources*, 2008, **185**, 876-880.

20.   Z.-G. Liu, S. Gao, J.-H. Ouyang and X.-L. Xia, *J. Alloy. Compd.*, 2010, **506**, 868-871.

21.   Z.-G. Liu, J.-H. Ouyang, K.-N. Sun and Y. Zhou, *Ceram. Int.*, 2012, **38**, 2935-2941.

22.   X.-L. Xia, S. Gao, Z.-G. Liu and J.-H. Ouyang, *Electrochim. Acta*, 2010, **55**, 5301-5306.

23.   T. Degen, M. Sadki, E. Bron, U. König and G. Nénert, *Powder Diffr.*, 2014, **29**, S13-S18.

24.   L. Vegard, *Zeitschrift für Physik*, 1921, **5**, 17-26.

25.   R. Shannon, *Acta Cryst. A*, 1976, **32**, 751-767.

26.   C. Chatzichristodoulou, P. Norby, P. Hendriksen and M. Mogensen, *J. Electroceram.*, 2015,
       34, 100-107.

27.   D. Marrocchelli, S. R. Bishop and J. Kilner, *J. Mater. Chem. A*, 2013, **1**, 7673-7680.

28.   F. N. Sayed, B. P. Mandal, D. Jain, C. G. N. S. Pillai and A. K. Tyagi, *J. Eur. Ceram. Soc.*,
       2012, **32**, 3221-3228.

29.   V. Thampi, P. R. Padala and A. N. Radhakrishnan, *New J. Chem.*, 2015, **39**, 1469-1476.

30.   R. W. B. N. Kjerulf-Jensen, and F. W. Poulsen, 2nd European Solid oxide fuel cell forum,
       1996.

31.   A. Banerji, V. Grover, V. Sathe, S. K. Deb and A. K. Tyagi, *Solid State Commun.*, 2009, **149**,
       1689-1692.

32.   J. R. McBride, K. C. Hass, B. D. Poindexter and W. H. Weber, *J. Appl. Phys.*, 1994, **76**,
       2435-2441.

33.   L. Li, F. Chen, J.-Q. Lu and M.-F. Luo, *J. Phys. Chem. A*, 2011, **115**, 7972-7977.

34.   B. P. Mandal, A. Banerji, V. Sathe, S. K. Deb and A. K. Tyagi, *J. Solid State Chem.*, 2007,
       180, 2643-2648.

35.   C. Wan, Z. Qu, A. Du and W. Pan, *J. Am. Ceram. Soc.*, 2011, **94**, 592-596.

36. T. Moriga, S. Emura, A. Yoshiasa, S. Kikkawa, F. Kanamaru and K. Koto, *Solid State Ionics*, 1990, **40–41, Part 1**, 357-361.

37. N. J. Hess, B. D. Begg, S. D. Conradson, D. E. McCready, P. L. Gassman and W. J. Weber, *J. Phys. Chem. B*, 2002, **106**, 4663-4677.

38. B. C. Chakoumakos, *J. Solid State Chem.*, 1984, **53**, 120-129.

39. L. Minervini, R. W. Grimes and K. E. Sickafus, *J. Am. Ceram. Soc.*, 2000, **83**, 1873-1878.

40. C. K. A. M. D. F. K. S. N. A. K. C. S. M. Y. X. J. Wu, *Phys. Rev. B*, 2003, **67**, 092508.

41. S. K. Mohanlal, *J. Phys. C: Solid State Phys.*, 1979, **12**, L651-L653.

42. D. R. Lide, ed., *CRC Handbook of Chemistry and Physics*, 2005.

43. A. D. Arulsamy, *Ann. Phys.*, 2011, **326**, 541-565.

44. Z. G. Liu, J. H. Ouyang and K. N. Sun, *Fuel Cells*, 2010, **10**, 1050-1056.

45. I. M. Hodge, M. D. Ingram and A. R. West, *J. Electroanal. Chem.*, 1976, **74**, 125-143.

46. P. Sarkar and P. S. Nicholson, *J. Am. Ceram. Soc.*, 1989, **72**, 1447-1449.

47. A. K. Baral and V. Sankaranarayanan, *Appl. Phys. Lett.*, 2009, **94**, 074101.

48. J. M. Réau, S. Rossignol, B. Tanguy, J. M. Rojo, P. Herrero, R. M. Rojas and J. Sanz, *Solid State Ionics*, 1994, **74**, 65-73.

49. K. P. Padmasree, D. K. Kanchan and A. R. Kulkarni, *Solid State Ionics*, 2006, **177**, 475-482.

50. A. K. Jonscher, *Nature*, 1977, **267**, 673-679.

51. J. García-Barriocanal, K. J. Moreno, G. Mendoza-Suárez, A. F. Fuentes, J. Santamaría and C. León, *J. Non-Cryst. Solids*, 2005, **351**, 2813-2818.

52. K. Moreno;, G. Mendoza-Suárez;, A. Fuentes;, J. García-Barriocanal; and C. L. J. Santamaria, *Phys. Rev. B*, 2005, **71**, 132301-132301-132304.

53. J. Garcia-Barriocanal, A. Rivera-Calzada, M. Varela, Z. Sefrioui, M. R. Díaz-Guillén, K. J. Moreno, J. A. Díaz-Guillén, E. Iborra, A. F. Fuentes, S. J. Pennycook, C. Leon and J. Santamaria, *Chem. Phys. Chem.*, 2009, **10**, 1003-1011.